geosciences

MDPI

Communication

Measurement and Modeling Air Quality Impacts of Dust Emissions from Unpaved Roads in Tuxtla Gutierrez, Chiapas

Emmanuel Díaz-Nigenda [1], John Tatarko [2,*], Horacio Morales-Iglesias [1], Zuleyma Hernández Méndez [1], Williams Vázquez Morales [1] and Miguel Angel Alatorre-Ibargüengoitia [1]

[1] Instituto de Investigación en Gestión de Riesgos y Cambio Climático, Universidad de Ciencias y Artes de Chiapas, Tuxtla Gutiérrez, Chiapas 29039, Mexico; emmanuel.diaz@unicach.mx (E.D.-N.); horacio.morales@unicach.mx (H.M.-I.); zuleymachernandez@gmail.com (Z.H.M.); williams.vazquez@unicach.mx (W.V.M.); miguel.alatorre@unicach.mx (M.A.A.-I.)

[2] USDA-ARS Rangeland Resources and Systems Research Unit, Fort Collins, CO 80526, USA

* Correspondence: John.Tatarko@ars.usda.gov; Tel.: +1-970-492-7320

Received: 12 June 2018; Accepted: 24 July 2018; Published: 30 July 2018

Abstract: Dust emissions from unpaved roads are one of the main pollutants affecting air quality around the world. As part of initial air quality studies in Tuxtla Gutiérrez (TGZ), Chiapas, Mexico, urban aeolian emission events from unpaved roads and simple meteorological inputs were measured in February 2014 at two different sites located within the city to characterize emissions for representative road conditions and to produce Industrial Source Complex (ISC3) model inputs. Emissions of particulate matter of aerodynamic diameter less than 10 μm (PM_{10}) were determined for eight wind erosion events. PM_{10} concentrations were measured downwind from sites using a Minivol sampler during February and March 2014. Three high PM_{10} concentration scenarios, associated with unstable conditions generated by cold fronts (CF) were selected to simulate dust plume dispersion to identify impacted areas. Results show that unpaved roads represent a potential source of dust that affect air quality of urban regions; in this study generating emissions $\geq 1.92 \times 10^{-3}$ g·m^{-2}·s^{-1} when winds ≥6 m·s^{-1} were present. Air pollution events that exceed the Mexico national standard for 24-h average PM_{10} concentration (≥75 μg·m^{-3}) were observed, impacting different areas in the city, representing a risk to human health. This demonstrates the influence of CF over southern Mexico, generating high PM_{10} concentrations in urban regions.

Keywords: wind erosion; dust particles; cold fronts; PM_{10}

1. Introduction

Mineral dust emissions are one of the main pollution sources that affect air quality around the world [1] and also have important implications on human health and visibility [2–7]. Inhalable particulates have been found to cause adverse effects on respiratory health and contribute to excess mortality [8–10]. Dust emissions are generated when vehicles transit over unprotected soils [11–13] causing air quality impacts affecting human health. Jazcilevich et al. [14] developed a stochastic model to estimate human exposure to emissions from the resuspension of road dust due to moving vehicles. They found that children experience a high risk when they are exposed to this activity. Other studies have shown the contribution of bare soils to air pollution where wind erosion is the main natural phenomenon affecting the emissions of dust particles. Vega et al. [15] have shown that the dry Lake of Texcoco is still a dust source that affects air quality in the north-east of Mexico City.

Using receptor models, Múgica et al. [16] showed that during the campaign Megacities Initiative: Local and Global Research Observations (MILAGRO), bare soils were one of the most important particulate sources, emitting up to 26% of the fine particles in some areas of Mexico City [17]. Using the Multiscale Climate and Chemistry Model (MCCM) and the Wind Erosion Prediction System (WEPS) model, Díaz-Nigenda et al. [18] studied four different air pollution episodes showing that wind erosion is a major cause of high PM_{10} concentrations over Mexico City. Hamidi et al. [19] studied the severe dust event of 3–8 July 2009 in the Middle East using the Weather Research Forecasting with the Chemistry Model coupled to a Dust Model (WRF–DuMo), showing that soil salt content plays an important role in dust emissions affecting air quality over different cities along Asia. Using the CHIMERE model with an offline coupling of the WRF model, Beegum et al. [20] simulated the aerosol optical depths over the Arabian Peninsula desert. Schwartz et al. [4] analyzed historical data of PM_{10} concentration, meteorology, and daily deaths from six different U.S. cities and suggested that increase in human morbidity and mortality is related to increments in PM_{10} concentrations. Laden et al. [21] found a consistent association between increments of PM_{10} concentrations (~10 $\mu g \cdot m^{-3}$) and the weighted mean percent change in daily mortality (~0.8%). For the effects of visibility, Hagen and Skidmore [5] established that wind erosion suspends enough particulates to create visibility hazards near highways and airports, while Chepil and Woodruff [22] also indicated that higher particle concentrations represent lower visibility. In Mexico, Jáuregui [23–25] explained the presence of dust storms affecting the visibility and air quality over Mexico City since 1920.

The application of a computational model can help in the identification of impacted areas by air pollutants. The Industrial Source Complex (ISC3) model [26] can be used to simulate the transport and deposition of dust particles considering local meteorological conditions. Given its modeling attributes, Etyemezian et al. [12] used the ISC3 model to simulate dust plumes generated from unpaved roads as a result of mechanical action of vehicle movements under different atmospheric stability and soil surface conditions. They found that the model could approximate the shape of a dust plume, however, variations in PM_{10} concentrations could not be reproduced as the measured data indicated. Qiu and Pattey [27] calculated PM_{10} emissions from spring wheat harvest applying a tracer technique. They used the ISC3 model to validate their results establishing that PM_{10} emissions generated by the model are comparable to those obtained using a gas tracer. Lazo et al. [28] determined hourly and daily sulphur dioxide (SO_2) concentrations applying the ISC3 model in an industrial city in Chile, establishing that the model is sensitive to wind speed and wind direction variations. To analyze human exposure to dust emissions generated by a composting site, Chalvatzaki et al. [29] evaluated ISC3 simulated PM_{10} concentrations associated to dispersion. They modelled piles in open storage yards of a municipal solid waste composting site as an area source using the ISC3 model, and observed that PM_{10} concentrations respond to variations in friction velocity, pile height and receptor height. In Mexico, López-Martínez and Gutiérrez-Lujú [30] applied the ISC3 model to evaluate the environmental impact by SO_2 dispersion over an industrial region in northern Mexico, identifying impacted areas by high SO_2 concentration.

Direct emission from wind erosion, as well as the transit of vehicles, also plays an important role in unpaved roads impacting downwind air quality. Dust plumes are often noticed over these sources when wind speeds are high enough [31,32]. Unpaved roads are long areas prone to wind erosion and can be considered as potential sources of dust particles affecting urban air quality and visibility during the dry season, representing an environmental risk for human health. The ability to model emissions and paths of PM_{10} could provide a planning tool for targeting source areas for dust control measures. Such a tool will also provide a means to evaluate potential health impacts to vulnerable populations downwind such as schools, hospitals, and the public in general.

Although dust generated by vehicle traffic on unpaved roads can be a significant source of particulates [11,12,33], direct emission and transport from urban unpaved road surfaces has had limited study. In this preliminary study, we quantified PM_{10} emissions by wind erosion from unpaved roads as affected by high wind intensities generated by entrances of cold front (CF) events over the

south-east of Mexico. The emissions also provided inputs for ISC3 simulations. The ISC3 model was applied to simulate the dispersion to define the impacted area along Tuxtla Gutiérrez (TGZ). This study was implemented with two main objectives: (1) to quantify dust emissions from unpaved roads; and (2) to model PM_{10} dispersion and concentrations over the city.

2. Methods

2.1. Study Site

TGZ (16°45′ N, 93°06′ W) is located in the south-east of Mexico and in the central region of Chiapas comprising an area of 334.61 km^2 at an elevation of 522 m above sea level (masl) (see Figure 1). This is a tropical zone with mean annual precipitation oscillating from 900 to 1200 mm·$year^{-1}$ [34] and surrounding areas consisting of forests. From November to the middle of March, the region is influenced by CF entrances over southern Mexico, which generate high wind intensities (up to 10 m·s^{-1}) coming from the west and north-west. The presence of two natural barriers, Mactumatzá Hill at the south and geological formations of the Cañón del Sumidero National Park at the north, both with elevations above 1000 masl, influence the prevailing wind direction and subsequent dispersion of air pollutants affecting the TGZ air quality. Agricultural areas outside of the city have been subjected to strong social pressure due to urban expansion generating unpaved street layouts for new human settlements. When soil aggregates and crusts are crushed by vehicle traffic, the content of loose soil material increases, causing an increase in soil susceptibility to wind erosion [11,35]. The presence of high wind speeds yields fugitive dust emissions impacting the region.

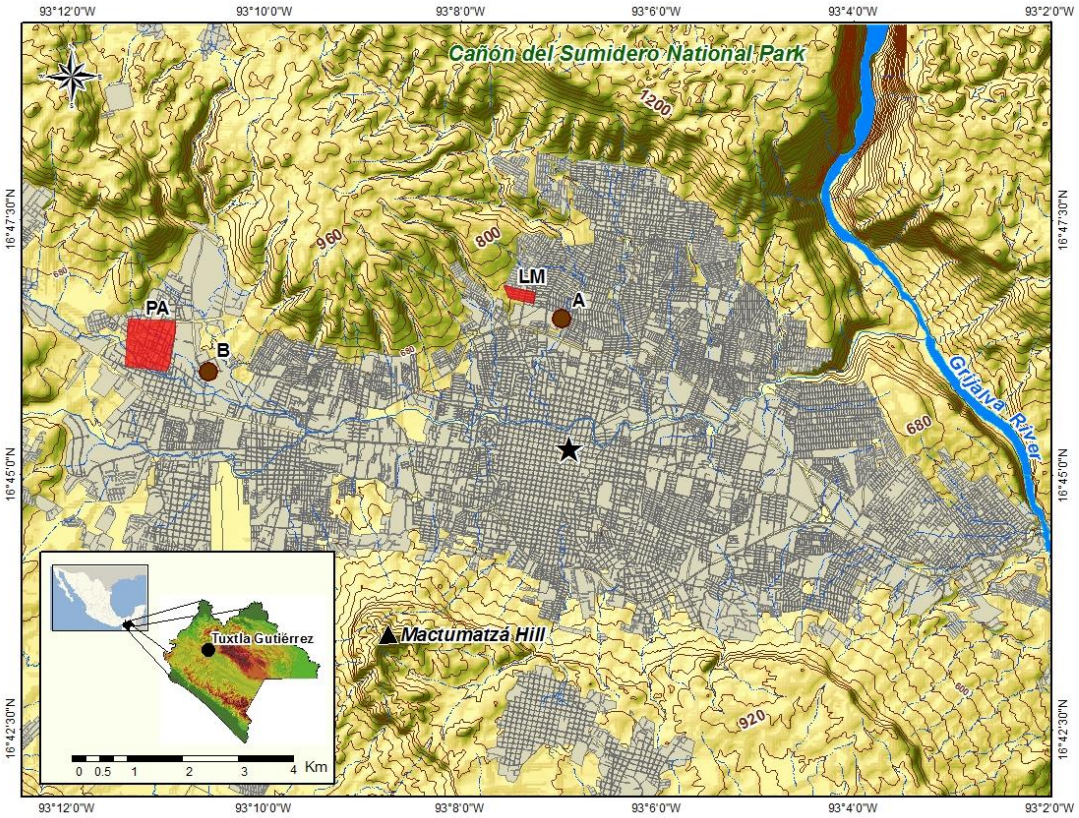

Figure 1. Sites selected in Tuxtla Gutiérrez (TGZ) to quantify emissions from unpaved roads are represented by red polygons and refer to Lajas Maciel (LM) and Plan de Ayala (PA). A and B represents points for monitoring PM_{10} concentration. The central part of the city is represented by ★. The blue lines represent the presence of rivers and streams. The brown slight lines represent elevation in meters above sea level.

2.2. Field Campaign

In order to quantify the dust emissions, a tower with five Big Spring Number Eight (BSNE) sediment catchers [36] was installed in 2014 for approximately four hours (i.e., 14:00 to 18:00 h) each day over unpaved roads during 12 February in the north at Lajas Maciel and during 21 February in the west at Plan de Ayala areas of TGZ (see Figures 1 and 2, Table 1). Although unpaved roads in the city are common, these sites were selected considering their orientation relative to prevailing wind direction and soil surface conditions of roads that are representative of places located around the city. Road emission measurements were only taken when the observed winds were within approximately ±10 degrees to the road direction. Table 2 lists some soil parameters obtained from soil sample analysis as well as some site characteristics. The roads in this study were considered source unlimited for fine loose particles given the frequent traffic that grind surfaces into new source material.

Table 1. Area of openings and height of each Big Spring Number Eight (BSNE) sediment catcher. The BSNE tower arrangement is diagrammed to the left.

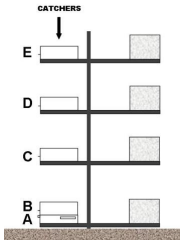

Catcher Location	Opening L × H (cm)	Height (m)	
		Lajas Maciel	Plan de Ayala
E	2 × 5	2.10	2.40
D		1.40	1.60
C		0.70	1.00
B		0.13	0.24
A	2 × 1	0.10	0.14

Table 2. Soil parameters and characteristics from the study sites.

Parameter	Site	
	Lajas Maciel	Plan de Ayala
Sand content (%)	64.1	70.8
Silt content (%)	12.0	10.3
Clay content (%)	23.9	19.0
Bulk density ($g \cdot cm^{-3}$)	1.4	1.6
Saltation size material content (%)	25.1	35.1
Suspension size material content (%)	5.9	6.3
PM_{10} content (%)	0.3	1.2
Slope (degrees)	12	7
Road width (m)	6	10
Distance up wind (m)	70	100

Primary particle size at each site was determined following the specifications established in NOM-021-SEMARNAT-2000 [37] which is based on the Bouyoucos method. Bulk density of loose surface material was determined using a 10 mL test tube [38]. Granulometry analysis of undispersed samples was made using sieves with openings of 9.5, 3.35, 2.0, 1.4, 1.0, 0.71, 0.5, 0.35, 0.25, 0.18, 0.125, 0.075 and 0.037 mm according to ASTM D422/63 [39]. PM_{10} source available for site emissions was approximated using a polynomial extrapolation from the granulometry analysis according to Wachecka-Kotkowska and Kotkowski [40].

Figure 2. Equipment installation over unpaved roads. (**a**) Lajas Maciel. (**b**) Plan de Ayala.

One Davis meteorological station (Davis Instruments, Hayward, CA, USA), model Vantage Vue (VV) with anemometer at 1 m height was installed together with BSNE catchers. Thus, every time the suspension of material was observed, the instant maximum wind speed was recorded in the station console. The equipment array was able to generate data about wind speed over the soil surface during different events. We defined a wind erosion event similar to Feng and Sharratt [41] where wind velocity exceeding the threshold for >20 consecutive seconds and terminated when the velocity was lower than the threshold for greater than 10 min. Based on this definition, a total of eight events were observed, and their associated sediment fluxes were calculated according to the expression presented in van Donk and Skidmore [42,43] and van Donk et al. [44]:

$$q(z) = a(z+1)^b \tag{1}$$

where $q(z)$ is sediment flux (kg·m^{-2}), z is the height of sampler opening above the soil surface (m), and a and b are fitting parameters considering the height and the mass collected by each BSNE catcher and vary for each storm event.

The discharge of sediments passing the BSNE catchers were then determined integrating Equation (1) from 0 to 2.5 m considering the highest BSNE catcher position (see Table 1):

$$Q = \int_0^{2.5} q(z)dz = \int_0^{2.5} a(z+1)^b dz = \frac{a}{b+1}[(2.5+1)^{b+1} - 1] \tag{2}$$

where Q is sediment discharge (kg·m^{-1}). It should be noted that we were interested in quantifying emissions generated only by natural wind action so when traffic was present, the catchers were covered to avoid mechanical contribution.

Similar to Hagen [45], the sediment discharge is divided by the distance to upwind limit to a non-erodible area to provide an approximation of soil loss per unit area of the unpaved road (see Table 2). Considering that an efficiency between 10 and 25 percent for PM_{10} dust emissions has been observed in BSNE sediment catchers [46,47], a mean value (17.5%) was used in this study.

Based on the sediment discharge, the soil loss and the mean efficiency value, the PM_{10} emissions were estimated according to Equation (3):

$$E_{PM10} = \frac{(Q)(\varepsilon)}{(d)(t)} \times 1000 \quad (3)$$

where E_{PM10} is PM10 emissions ($g \cdot m^{-2} \cdot s^{-1}$), ε is the catcher efficiency, d is the distance to upwind limit (m) and t (s) is the duration of the event (i.e., mean value of 10 s).

PM_{10} emissions were related to the high wind speed at which suspended material was observed (see Table 3). In this way linear regression equations were obtained correlating PM_{10} emissions with maximum wind speed from VV. These equations were used to approximate PM_{10} emissions under different scenarios (Figure 4).

TGZ air quality was monitored using a Minivol Portable Sampler (Airmetrics model TAS-5.0, Springfield, Oregon, USA) at a flow rate of 5 $L \cdot min^{-1}$ with a 10 µm impactor separator with PM_{10} collected on a 47 mm conditioned quartz fiber filter for gravimetric analysis. The Minivol sampler was installed at ~10 m height downwind from Lajas Maciel (15 February–1 March) and Plan de Ayala (3–15 March) in 2014. The locations of the Minivol sampler are shown in Figure 1. A Davis meteorological station model Vantage Pro2 (VP2) was installed at the same monitoring sites as the Minivol (Figure 3) to obtain wind directions and wind speeds to relate PM_{10} concentrations with probable sources.

Figure 3. PM_{10} monitoring stations at the study sites. (**a**) Site located downwind from Lajas Maciel. (**b**) Site located downwind from Plan de Ayala.

2.3. Model Application for Impacted Areas

The ISC3 model was used to simulate the dust plume dispersion to have an approximation of the impacted areas by PM_{10} along TGZ. The model is based on the straight-line, steady-state Gaussian plume equation and includes a wide range of options for modeling air quality impacts of pollution sources. Emission sources are categorized into four basic types of sources, i.e., point sources, volume sources, area sources, and open pit sources [26]. Considering representative roads in TGZ as area sources of PM_{10} discharge, in this work the ISC3 was used to calculate the ground-level concentration at a receptor located downwind of all or a portion of the source.

In order to identify the areas impacted by dust particles during days presenting high PM_{10} concentrations, meteorological and emission input files were created from the field campaign for the ISC3 model execution. The meteorological input file contained wind speed, wind direction, and

temperature mean hourly data which were obtained from VP2. Hourly high wind speeds from VP2 were used to create the dust emissions input file using linear regression equations previously obtained from field work data to approximate PM_{10} emissions from unpaved roads. Once the ISC3 model had been executed, the PM_{10} concentrations generated by the model were plotted to create the dust plume using the ordinary Kriging interpolation method in ArcGIS 10.0 [48].

3. Results and Discussion

3.1. Field Measurements

As can be seen in Table 2, surface soil samples of two sites were mainly composed of sand. According to particle size analysis, Plan de Ayala presented higher sand content (70.8%) than Lajas Maciel (64.1%). Conversely, clay and silt content were higher in Lajas Maciel (23.9 and 12.0% respectively) than in Plan de Ayala (19.0 and 10.3%, respectively). Bulk density results show that the value in Plan de Ayala was higher (1.6 g·cm^{-3}) than in Lajas Maciel (1.4 g·cm^{-3}). Lajas Maciel had roads with slopes slightly more pronounced than Plan de Ayala which were determined using a clinometer. As can be seen in Table 3, these differences may contribute to the discharge of sediments in Plan de Ayala being higher than in Lajas Maciel. Granulometry showed that there was a low natural PM_{10} content at the two sites, but saltation and suspension size material content were higher in Plan de Ayala than in Lajas Maciel. However, Mirzamostafa et al. [49] cited that abrasion of soil clods accounted for 14–27% additional suspension size material than available as loose erodible material in the soil. Hagen [50] also found that breakdown of saltating aggregates during erosion contributed on average, 4.9% of PM_{10} emissions greater than that originally present in the source material for a range of soils from nine western U.S. states.

Field aeolian emission events from unpaved roads were measured at sites in order to characterize emissions for representative road conditions in Lajas Maciel during 12 February and in Plan de Ayala during 21 February. The discharge of sediments and PM_{10} emissions were calculated from sediment collected in BSNE catchers installed over unpaved roads in two different sites in TGZ (see Table 3). Linear fits (LF) relating maximum observed wind speeds from VV and PM_{10} emissions are shown in Figure 4. The LF permitted us to know the quantity of PM_{10} emitted in different scenarios as a response to different values of wind speed. In this sense, the emission input file to simulate particulate dispersion during days with high PM_{10} concentration using the ISC3 model was created using LF and hourly high wind speed from VP2.

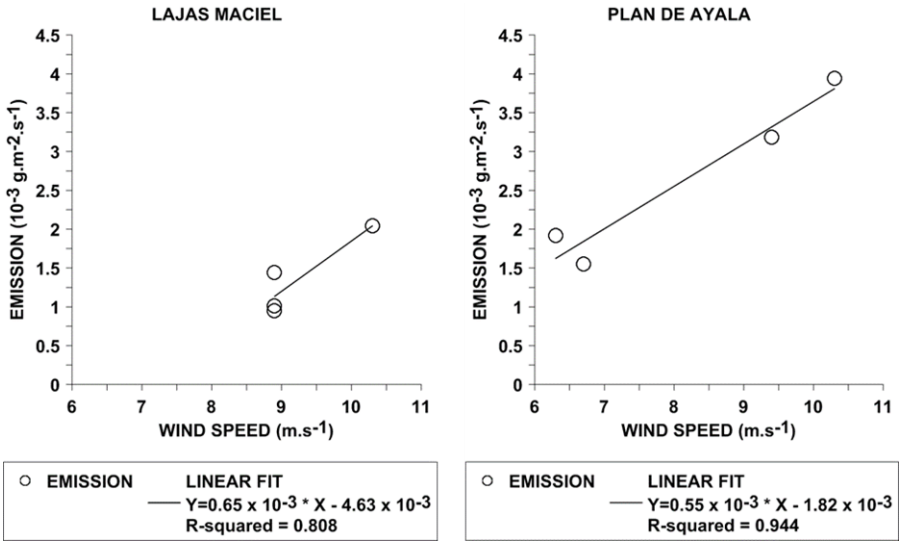

Figure 4. PM_{10} dust emissions from unpaved roads as affected by wind speed for 12 February at Lajas Maciel and 21 February 2014 at Plan de Ayala.

In Lajas Maciel (R^2 = 0.808) and Plan de Ayala (R^2 = 0.944) a positive linear trend was observed between PM_{10} emissions and high wind speeds. This is as expected due to near unlimited source of fine loose surface material which is characteristic of the many unpaved roads located around TGZ (Figure 4).

Wind erosion emissions were observed when wind speeds were $\geq$9 m·s^{-1} in Lajas Maciel. By comparison, in Plan de Ayala, the erosive process was initiated when surface wind speeds of $\geq$6 m·s^{-1} were present (Figure 4). These wind threshold differences could possibly be due to the greater content of erodible size source at Plan de Ayala (Table 2). Storm events at this site were also visually more intense. Considering the results obtained from the field work, dust emissions indicate not only the influence of high wind speeds (Figure 4) but also wind turbulence generated by soil surface conditions and street layouts (Figure 2).

Table 3. Discharge of sediments and calculated PM_{10} dust emissions from unpaved roads for eight wind events observed.

Site	Date	Event	Maximum Observed Wind Speed (m·s^{-1})	Discharge of Sediments (10^{-3} kg·m^{-1})	PM_{10} Emission (10^{-3} g·m^{-2}·s^{-1})
Lajas Maciel	12 February 2014	1	8.9	3.78	0.95
		2	10.3	8.17	2.04
		3	8.9	4.06	1.02
		4	8.9	5.78	1.45
Plan de Ayala	21 February 2014	1	9.4	18.18	3.18
		2	6.3	10.95	1.92
		3	6.7	8.86	1.55
		4	10.3	22.52	3.94

The Minivol measured the 24-h average PM_{10} concentration downwind from Lajas Maciel (15 February–1 March 2014) and Plan de Ayala (3–15 March 2014) (location of monitoring sites is shown in Figure 1). The highest PM_{10} concentration downwind from Lajas Maciel was observed during 27 February 2014 (1307 μg·m^{-3}) while high concentrations downwind from Plan de Ayala were observed during 8 March 2014 (114 μg·m^{-3}) and 13 March 2014 (63 μg·m^{-3}) when wind speeds and wind direction recorded by VP2 (see Figures 1 and 5) allowed the particulate transport to monitoring site. Note that the wind speeds on days associated with the entrances of CF exhibit a wider distribution (i.e., higher winds throughout the day) compared to adjacent days without a CF event. The wider distribution of wind speed during the CF event would result in greater total wind energy during the CF for driving the erosion and dust dispersion processes. Considering that the entrances of the CF during those days resulted in high winds in TGZ, the high measured PM_{10} concentrations on these days were associated with wind erosion phenomena on unpaved roads aligning with the wind direction.

Some peaks of PM_{10} concentrations were present with low measured wind speeds while low PM_{10} concentrations were present with high measured wind speeds (Figure 5). This may be attributed to minor variations in wind direction relative to the road direction, which would be expected to vary measured wind speeds and concentrations. In addition, discharge generated by vehicle traffic or by burning of garden waste near to the monitoring site during those days would affect concentrations.

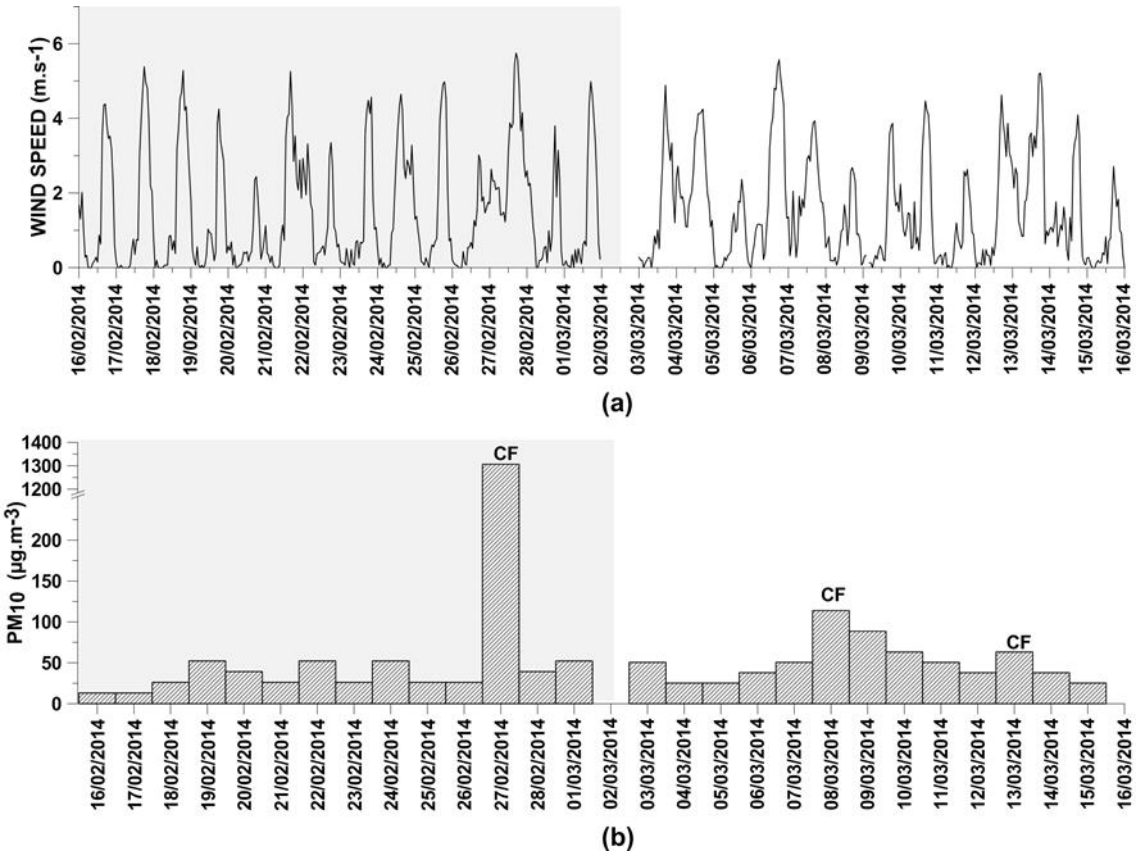

Figure 5. Mean hourly wind speeds calculated from 10 min measurements (**a**) and 24-h average PM_{10} concentration (**b**) during the monitoring campaign. The shaded part refers to winds and concentrations downwind from Lajas Maciel while the clear part refers to winds and concentrations downwind from Plan de Ayala. The notation CF refers to the entrance of a cold front event, characterized by greater than normal winds. Discontinuity in plot represents the day for change of location of equipment.

3.2. Simulations

The ISC3 model was applied to simulate the high PM_{10} concentration events and to identify areas impacted by dust particles. Mean hourly wind speed, wind direction, and temperature data from VP2 were used to define the meteorological input files of the model. PM_{10} emission input files were generated using hourly high wind speed from VP2 and applying the LF obtained from results of field work shown in Figure 4. The ISC3 model results were processed using the ordinary Kriging interpolation method in ArcGIS to generate dust plumes for 27 February and 8 and 13 March 2014, considering unpaved roads from Lajas Maciel and Plan de Ayala as area sources. As seen in Figure 5, these dates correspond to the entrance of cold front events, characterized by greater than normal winds associated with unstable conditions.

Observed PM_{10} concentration and those generated by the ISC3 model are shown in Table 4. As can be seen, the magnitude of PM_{10} concentrations were underestimated by the model for the 27 February 2014 event, however the model could reproduce the event. If other areas with similar characteristics to Lajas Maciel and located to the north of the monitoring site had been considered, the results from the ISC3 would have been similar to those observed during that day due to cumulative concentrations from overlap of adjacent plumes. PM_{10} concentrations were over-estimated by the model for 8 and 13 March, where the presence of tall vegetation (e.g., trees) and buildings around the monitoring site, represent natural barriers that affect the particles distribution over the site which is not seen by the model. This explains why the model generates a higher concentration than observed.

Table 4. Comparison of 24-h PM_{10} average concentrations between Minivol and Industrial Source Complex (ISC3) model during CF entrance events.

Date	PM_{10} ($\mu g \cdot m^{-3}$)	
	Minivol	ISC3
27 February 2014	1307	37
8 March 2014	114	177
13 March 2014	63	403

It should be noted that the US-EPA set their National Ambient Air Quality Standards for PM_{10} at 150 $\mu g \cdot m^{-3}$ of 24-h average concentration "to protect and enhance the quality of the Nation's air resources so as to promote the public health and welfare and the productive capacity of its population" [51]. The standard for PM_{10} in Mexico however was established by NOM-025-SSA1-2014 at 75 $\mu g \cdot m^{-3}$ of 24-h average concentration [52].

Figure 6 shows the simulated distribution of the PM_{10} dust plume coming from Lajas Maciel during 27 February 2014. The plume traveled from north-west to south-east of the city starting in Lajas Maciel. It can be seen that the monitoring site was affected by dust emissions. The high PM_{10} concentration reported by the Minivol sampler during 27 February 2014 (Figure 5) can be likely explained by the emissions coming from other bare areas that may be potential dust sources (e.g., other unpaved roads and bare land) located to the north of the monitoring site that were not considered in this study. Vehicle traffic could represent another important contribution of dust emissions affecting air quality according to Etyemezian et al. [12] and Kuhns et al. [13]. During this day, a PM_{10} concentration of 1307 $\mu g \cdot m^{-3}$ was obtained from the sampler, while a concentration of 37 $\mu g \cdot m^{-3}$ is shown by the modeled plume over the monitoring site (see Figure 7).

Surface distribution of the PM_{10} dust plume from Plan de Ayala for March 8th is shown in Figure 7. The plume affected mainly the north-western part of TGZ but meteorological conditions enhanced the dust transport to the central part of the city. The ISC3 model showed that PM_{10} concentrations at the monitoring site could be influenced by the emissions from unpaved roads located in Plan de Ayala. During this day the model reproduced a concentration of 177 $\mu g \cdot m^{-3}$ while the Minivol sampler reported 114 $\mu g \cdot m^{-3}$ (see Figures 5 and 7).

Figure 8 shows the surface distribution of the PM_{10} dust plume from Plan de Ayala for 13 March 2014. Variation in wind direction during the day generated two plumes that affected a large part of TGZ. The ISC3 model showed that PM_{10} concentrations at the monitoring site could be influenced by the emissions from unpaved roads located in Plan de Ayala. During this day the model reproduced a concentration of 403 $\mu g \cdot m^{-3}$ while the Minivol sampler reported 63 $\mu g \cdot m^{-3}$ (see Figures 5 and 8). Considering these results and the presence of tall vegetation and buildings around the monitoring site, it is likely that part of the population was exposed to particulate concentrations exceeding the maximum permissible values set in Mexico environmental standards [52].

The west part of the city is mainly affected by emissions coming from Plan de Ayala generating concentrations higher than the PM_{10} standard for Mexico (75 $\mu g \cdot m^{-3}$ of 24-h average concentration) [52] while the Central part of the city could be affected considering the prevailing wind direction. Emissions coming from Lajas Maciel affected mainly the north part of TGZ, but the central and east part could be affected as well. Considering the results during simulation days, emissions from Plan de Ayala impacted a larger population area with high PM_{10} concentrations than those from Lajas Maciel (Figures 6–8). This is a consequence of the wind speeds presented during those days and to the characteristic of sites affecting dust emissions as previously discussed (Figure 5 and Table 2). Considering the population density variation of TGZ and the impacted areas, emissions from Plan de Ayala represent a greater environmental risk for population health.

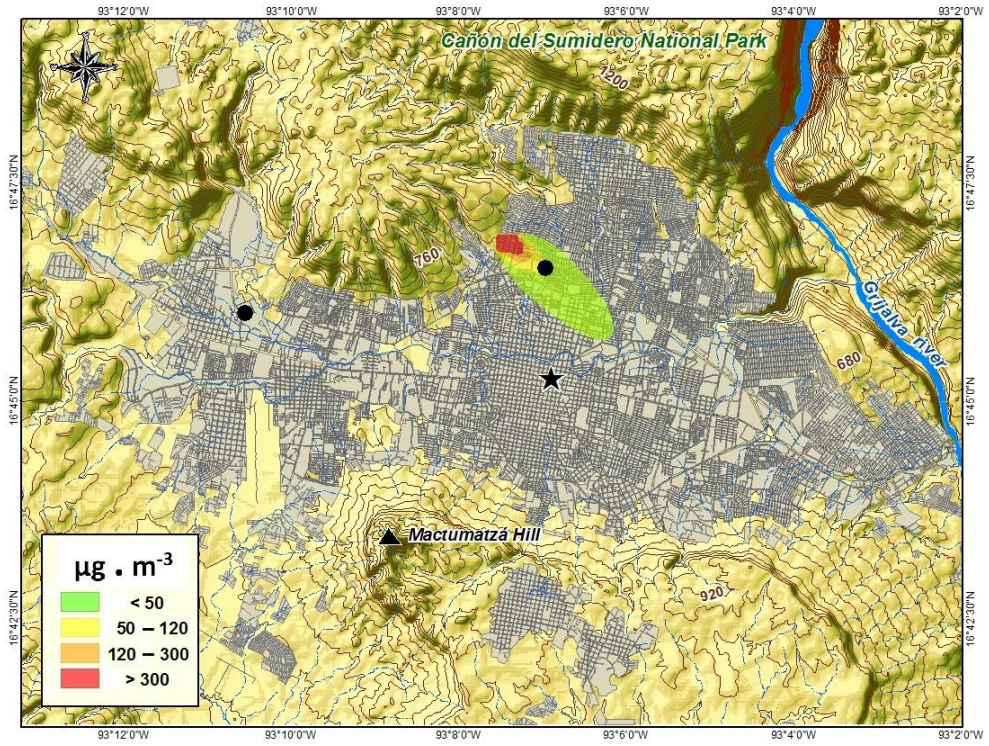

Figure 6. Dispersion of PM_{10} dust particles over TGZ as simulated by the ISC3 model. Plume originating from Lajas Maciel during February 27th, 2014. Points for Minivol monitoring PM_{10} concentration are represented by ●. The central part of the city is represented by ★.

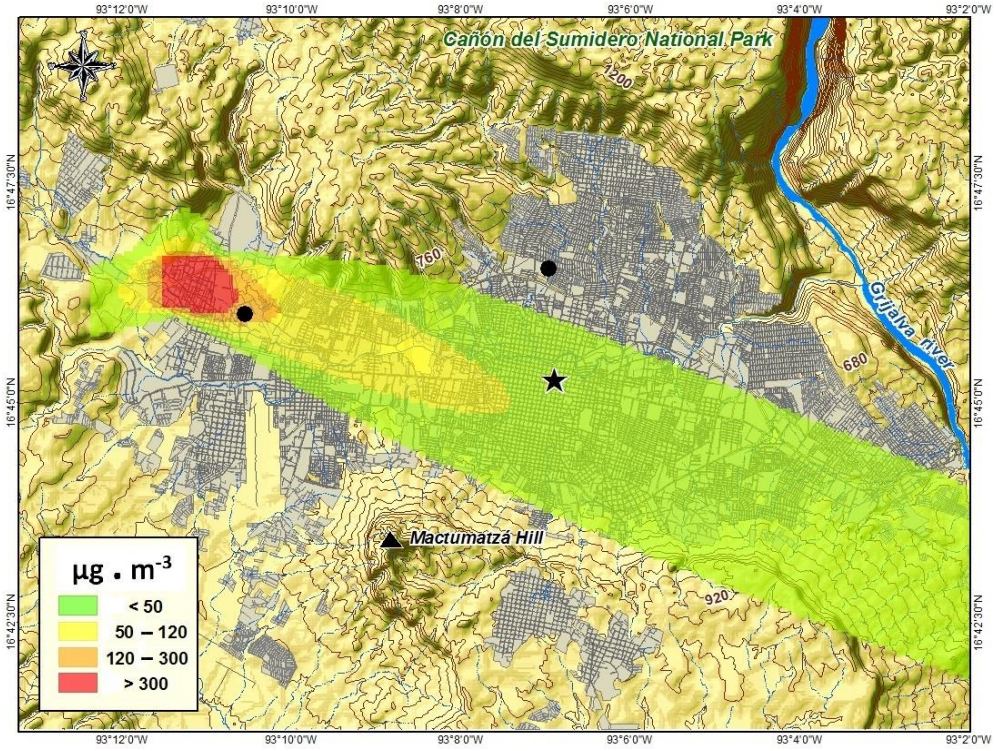

Figure 7. Dispersion of PM_{10} dust particles over TGZ as simulated by the ISC3 model. Plume originating from Plan de Ayala during March 8th, 2014. Points for Minivol monitoring PM_{10} concentration are represented by ●. The central part of the city is represented by ★.

In the current study, Lajas Maciel and Plan de Ayala were only two sites out of many settlements having unpaved roads within TGZ. There are many other sites with the same type of roads which means that it is very probable that PM_{10} concentrations and the extent of impacted areas over the city may be significantly greater than those generated by the model. In addition, the presence of burned or other bare areas along the city edge as well as forest fires could represent additional potential sources of PM_{10} that affect the air quality of TGZ and it is likely that some of these sources could have contributed to the high PM_{10} concentrations reported 27 February.

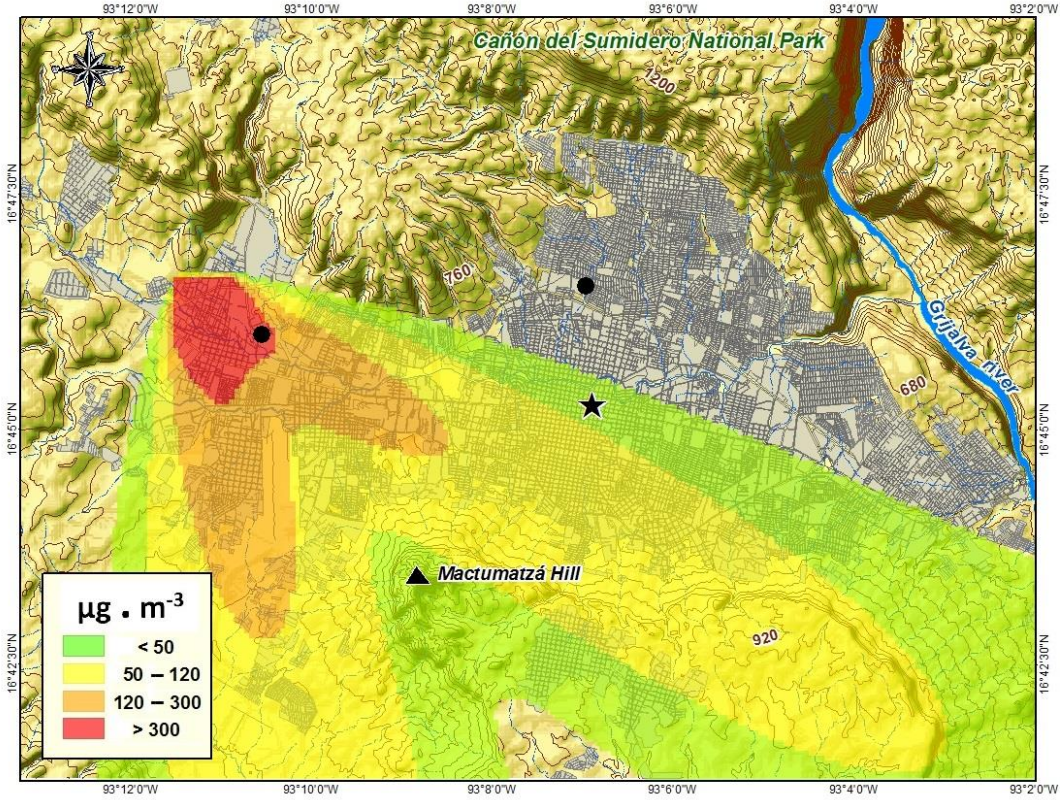

Figure 8. Dispersion of PM_{10} dust particles over TGZ as simulated by the ISC3 model. Plume originating from Plan de Ayala during 13 March 2014. Points for Minivol monitoring PM_{10} concentration are represented by ●. The central part of the city is represented by ★.

4. Conclusions

A preliminary field campaign was carried out to quantify dust emissions and parameterize the ISC3 model for two different sites within TGZ. Aeolian emission events from unpaved roads and simple meteorological inputs were measured at two different sites located within the city to characterize emissions for representative road conditions and to produce ISC3 model inputs. Emissions of PM_{10} were measured for eight wind erosion events.

Overall, results show that unpaved roads represent a potential source of dust that affects air quality of urban regions. In this study we found unpaved roads generated emissions $\geq 1.92 \times 10^{-3}$ g.m^{-2}·s^{-1} when winds ≥ 6 m·s^{-1} were observed. Air quality of this urban region was also affected as a result of high wind generated under unstable atmospheric conditions of CF, which resulted in at least one event with a measured PM_{10} concentration over 1300 µg·m^{-3}, which exceeds the Mexico national standard. Air pollution events that exceeded the Mexico national standard for PM_{10} (≥ 75 µg·m^{-3}) were observed, impacting different areas in the city, representing an environmental risk. Considering soil parameters and street layouts, emissions from Plan de Ayala were higher than those generated in Lajas Maciel. These results indicate that prioritizing dust controls (e.g., paving or application of dust

suppressants) on unpaved roads in those north-west parts of TGZ would provide greater reduction in PM_{10} exposures to the general population downwind to the south-east than applying controls to the south-east part of TGZ where winds will carry PM_{10} to relatively unpopulated areas. However, if paving activities are considered, it is necessary to evaluate materials that could be used to prevent other environmental problems such as urban heat island formation (e.g., low radiation adsorbing pavement) or flooding of low parts of the city during the rainy season due to surface water runoff (e.g., porous pavement).

Dust emissions from unpaved roads by wind erosion are less likely than those generated by mechanical action, but as this study indicates, they are no less important. In this sense, isolated dust emissions events from unpaved roads resulting from wind erosion can affect air quality of urban and even rural areas and can generate air pollution scenarios with PM_{10} concentration higher than established standards.

5. Future Research

The results of this study represent the beginning of air pollution research into the urban air quality of southern Mexico and show the need for air quality monitoring networks in such urban environments. Studies are needed that partition various sources like vehicle traffic, fires, burning of wood and coal in cooking or other activities, dust emissions from agricultural lands, fugitive emissions from construction activities, among others to determine their contribution to air quality in TGZ. During the field measurement portion of this study, there were only a few events where we observed both high winds that were along the direction of the road. Therefore, in order to improve modelling of dust emissions from unpaved roads, future research should include detailed measurements of source sites, measurements of more storm events, the effect of natural barriers on dust dispersion, as well as wind speed profiles at the eroding surface for friction velocity determination. More advanced models, such as WRF-CHEM, should also be used for better simulation of urban settings to understand the problem.

Considering the accelerated growth of TGZ and other areas in the region, the forecast of model emissions and dispersion paths of PM_{10} for new unpaved street layouts and other development for urban areas could represent an important tool for land planning. Impacts of PM_{10} on human health, dry deposition studies, traffic contributions, effect of turbulence generated by street layouts and roughness on dust emissions, the effect of the orientation of unpaved roads relative to wind direction and particle composition analysis are complementary areas of interest that are needed.

Author Contributions: Conceptualization, E.D.-N. and J.T.; Methodology, E.D.-N., H.M.-I., Z.H.M., W.V.M. and M.A.A.-I.; Implementation of the Dispersion Model (software), E.D.-N., Z.H.M. and W.V.M.; formal analysis, E.D.-N. and J.T.; Writing-Original Draft Preparation, E.D.-N., J.T. and M.A.A.-I.; Visualization, E.D.-N., J.T. and H.M.-I.; Project Administration and Funding Acquisition, E.D.-N.; and Implementation of Geographical Information System, H.M.-I.

Funding: This work was supported by the Program for Faculty Development (PRODEP) from Department of Public Education of Mexico (Grant number: UNICACH-PTC-053).

Acknowledgments: The authors are grateful to Arón Jazcilevich from CCA-UNAM for suggestions on improving the manuscript, Mariana Zavaleta and Kate Meza for providing support in processing information, and acknowledge the support provided by "Laboratorio de Ciencias de la Tierra y Medio Ambiente" and "Laboratorio Académico de Investigación y Salud Ambiental" from "Universidad de Ciencias y Artes de Chiapas".

Conflicts of Interest: The authors declare no conflicts of interest.

References

1. Choobari, O.A.; Zawar-Reza, P.; Sturman, A. The global distribution of mineral dust and its impacts on the climate system: A review. *Atmos. Res.* **2014**, *138*, 152–165. [CrossRef]
2. Ostro, B.D.; Hurley, S.; Lipsett, M.J. Air pollution and daily mortality in the Coachella Valley, California: A study of PM_{10} dominated by coarse particles. *Environ. Res.* **1999**, *81*, 231–238. [CrossRef] [PubMed]

3. Pope, C.A.; Thun, M.J.; Namboodiri, M.M.; Dockery, D.W.; Evans, J.S.; Speizer, F.E.; Heath, C.W., Jr. Particulate air pollution as a predictor of mortality in a prospective study of U.S. adults. *Am. J. Respir. Crit. Care Med.* **1995**, *151*, 669–674. [CrossRef] [PubMed]
4. Schwartz, J.; Dockery, D.; Neas, L. Is Daily Mortality Associated Specifically with Fine Particles? *J. Air Waste Manag. Assoc.* **1996**, *46*, 927–939. [CrossRef] [PubMed]
5. Hagen, L.J.; Skidmore, E.L. Wind Erosion and Visibility Problems. *Trans. ASAE* **1977**, *20*, 898–903. [CrossRef]
6. Gillette, D.A. Dust production by wind erosion: Necessary conditions and estimates of vertical fluxes of dust and visibility reduction by dust. In *Physics of Desertification*; El-Baz, F., Hassan, M.H.A., Eds.; Martinus Nijhoff Publisher: Dordrecht, The Netherlands, 1986; pp. 361–371.
7. Calderón-Garcidueñas, L.; Gónzalez-Maciel, A.; Reynoso-Robles, R.; Delgado-Chávez, R.; Mukherjee, P.; Kulesza, R.; Torres-Jardón, R.; Ávila-Ramírez, J.; Villarreal-Ríos, R. Hallmarks of Alzheimer disease are evolving relentlessly in Metropolitan Mexico City infants, children and young adults. APOE4 carriers have higher suicide risk and higher odds of reaching NFT stage V at $\leq$ 40 years of age. *Environ. Res.* **2018**, *164*, 475–487. [CrossRef] [PubMed]
8. Penttinen, P.; Timonen, K.L.; Tiittanen, P.; Mirme, A.; Ruuskanen, J.; Pekkanen, J. Ultrafine particles in urban air and respiratory health among adult asthmatics. *Eur. Respir. J.* **2001**, *17*, 428–435. [CrossRef] [PubMed]
9. Kanatani, K.T.; Ito, I.; Al-Delaimy, W.K.; Adachi, Y.; Mathews, W.C.; Ramsdell, J.W. Desert dust exposure is associated with increased risk of asthma hospitalization in children. *Am. J. Respir. Crit. Care Med.* **2010**, *182*, 1475–1481. [CrossRef] [PubMed]
10. Goudie, A.S. Desert dust and human health disorders. *Environ. Int.* **2014**, *63*, 101–113. [CrossRef] [PubMed]
11. Gillies, J.A.; Watson, J.G.; Rogers, F.; DuBois, D.; Chow, J.C.; Langston, R.; Sweet, J. Long-Term Efficiencies of Dust Suppressants to Reduce PM_{10} Emissions from Unpaved Roads. *J. Air Waste Manag. Assoc.* **1999**, *49*, 3–16. [CrossRef] [PubMed]
12. Etyemezian, V.; Ahonen, S.; Nikolic, D.; Gillies, J.; Kuhns, H.; Gillette, D.; Veranth, J. Deposition and Removal of Fugitive Dust in the Arid Southwestern United States: Measurements and Model Results. *J. Air Waste Manag. Assoc.* **2004**, *54*, 1099–1111. [CrossRef] [PubMed]
13. Kuhns, H.; Gillies, J.; Etyemezian, V.; Dubois, D.; Ahonen, S.; Nikolic, D.; Durham, C. Spatial Variability of Unpaved Road Dust PM_{10} Emission Factors near El Paso, Texas. *J. Air Waste Manag. Assoc.* **2005**, *55*, 3–12. [CrossRef] [PubMed]
14. Jazcilevich, A.; Wellens, A.; Siebe, C.; Rosas, I.; Bornstein, R.; Riojas-Rodríguez, H. Application of a stochastic vehicular wake erosion model to determine $PM_{2.5}$ exposure. *Aeolian Res.* **2012**, *4*, 31–37. [CrossRef]
15. Vega, E.; Reyes, E.; Sánchez, G.; Ortíz, E.; Ruíz, M.; Chow, J.; Watson, J.; Edgerton, S. Basic statistics of $PM_{2.5}$ and PM_{10} in the atmosphere of Mexico City. *Sci. Total Environ.* **2002**, *287*, 167–176. [CrossRef]
16. Mugica, V.; Ortiz, E.; Molina, L.; De Vizcaya-Ruiz, A.; Nebot, A.; Quintana, R.; Aguilar, J.; Alcántara, E. PM composition and source reconciliation in Mexico City. *Atmos. Environ.* **2009**, *43*, 5068–5074. [CrossRef]
17. MCE2. Megacities Initiative: Local and Global Research Observations. Molina Center for Energy and the Environment, 2009. Available online: www.mce2.org/es/campanas/zmvm-2006 (accessed on 26 May 2018).
18. Díaz-Nigenda, E.; Tatarko, J.; Jazcilevich, A.; García, A.; Caetano, E.; Ruíz-Suárez, G. A modeling study of Aeolian erosion enhanced by surface wind confluences over Mexico City. *Aeolian Res.* **2010**, *2*, 143–157. [CrossRef]
19. Hamidi, M.; Reza, M.K.; Shao, Y. Numerical simulation of dust events in the Middle East. *Aeolian Res.* **2014**, *13*, 59–70. [CrossRef]
20. Beegum, S.N.; Gherboudj, I.; Chaouch, N.; Couvidat, F.; Menut, L.; Ghedira, H. Simulating aerosols over Arabian Peninsula with CHIMERE: Sensitivity to soil, surface parameters and anthropogenic emission inventories. *Atmos. Environ.* **2016**, *128*, 185–197. [CrossRef]
21. Laden, F.; Neas, L.; Dockery, D.; Schwartz, J. Association of Fine Particulate Matter from Different Sources with Daily Mortality in Six U.S. Cities. *Environ. Health Perspect.* **2000**, *108*, 941–947. [CrossRef] [PubMed]
22. Chepil, W.S.; Woodruff, N.P. Sedimentary characteristics of dust storms. Part II. Visibility and dust concentration. *Am. J. Sci.* **1957**, *255*, 104–114. [CrossRef]
23. Jáuregui, E. La erosión eólica en los suelos vecinos al lago de Texcoco [Wind erosion in neighboring soils of Lake of Texcoco]. *Ingeniería Hidráulica en México* **1971**, *XXV-2*, 103–117.
24. Jáuregui, E. Variaciones de largo periodo de la visibilidad en la Ciudad de México [Long period variations of visibility in Mexico City]. *Geofísica Internacional* **1983**, *22–23*, 251–275.

25. Jáuregui, E. The dust storms of Mexico City. *Int. J. Climatol.* **1989**, *9*, 169–180. [CrossRef]
26. U.S. Environmental Protection Agency (US-EPA). *User's Guide for the Industrial Source Complex (ISC3) Dispersion Models, Volume I—User Instruction*; EPA-454/B-95-003a; U.S. Environmental Protection Agency: Research Triangle Park, NC, USA, 1995.
27. Qiu, G.; Pattey, E. Estimating PM_{10} emissions from spring wheat harvest using an atmospheric tracer technique. *Atmos. Environ.* **2008**, *42*, 8315–8321. [CrossRef]
28. Lazo, P.; Curé, M.; Gaete, H. Modelación de la dispersión de Anhídrido Sulfuroso en la comuna de Puchuncaví utilizando el programa ISC3 [Modelling of sulphur anhydride dispersion in Puchuncaví city using the ISC3 model]. Ingeniare. *Revista Chilena de Ingeniería.* **2006**, *14*, 229–237.
29. Chalvatzaki, E.; Aleksandropoulou, V.; Glytsos, T.; Lazaridis, M. The effect of dust emissions from open storage piles to particle ambient concentration and human exposure. *Waste Manag.* **2012**, *32*, 2456–2468. [CrossRef] [PubMed]
30. López-Martínez, J.; Gutiérrez-Lujú, S. Comparación de los datos de dispersión de bióxido de azufre y otros contaminantes en la atmósfera, obtenidos experimentalmente y por simulación usando el modelo ISC3 [Data comparison of sulphur dioxide dispersion and other pollutants in the atmosphere, obtained experimentally and by simulation using the ISC3 model]. *Tecnología Ciencia y Educación* **1999**, *14*, 10–18.
31. Návar, J.; Treviño, E. Estimating Tonnage of Soil Particles which Potentially Contribute to Air Pollution in the Metropolitan Area of Monterrey, Mexico. *Terra* **1998**, *16*, 21–31.
32. Watson, J.G.; Chow, J.C.; Pace, T.G. Fugitive dust emissions. In *Air Pollution Engineering Manual*; Davis, T.W., Ed.; John Wiley & Sons, Inc.: New York, NY, USA, 2000; pp. 117–135.
33. Kavouras, I.; DuNois, D.W.; Nikolich, G.; Corral Avittia, A.Y.; Etyemezian, V. Particulate dust emission factors from unpaved roads in the U.S.–Mexico border semi-arid region. *J. Arid Environ.* **2016**, *124*, 189–192. [CrossRef]
34. CEIEG. Comité Estatal de Información Estadística y Geográfica, Gobierno del Estado de Chiapas [State Committee of Statistical and Geographic Information, Government of the State of Chiapas]. 2017. Available online: www.ceieg.chiapas.gob.mx/perfiles/ (accessed on 26 May 2018).
35. U.S. Environmental Protection Agency (US-EPA). *AP 42, Fifth Edition Compilation of Air Pollutant Emission Factors, Volume 1: Stationary Point and Area Sources*; U.S. Environmental Protection Agency: Research Triangle Park, NC, USA, 1995.
36. Fryrear, D.W.; Stout, S.E.; Hagen, L.J.; Vories, E.D. Wind erosion: Field measurement and analysis. *Trans. ASAE* **1991**, *34*, 155–160. [CrossRef]
37. Prieto Méndez, J.; Prieto García, F.; Acevedo Sandoval, O.; Méndez Marzo, M. Correlation of moisture, pH and zeta potential (ζ) in sandy-clay-loam soils of the southern state of Hidalgo, Mexico. *Acta Montanistica Slovaca Ročník* **2013**, *18*, 17–25.
38. Delgadillo Ramírez, M.; Quechulpa Montalvo, S. *Manual de Monitoreo de carbono en Sistemas agroforestales [Handbook for Monitoring Carbon in Agroforestry Systems]*; Comisión Nacional Forestal: Mexico, D.F., Mexico; AMBIO S.C. de R.L.: Chiapas, Mexico, 2006.
39. ASTM D422/63. *Standard Test Method for Particle-Size Analysis of Soils*; ASTM International: West Conshohocken, PA, USA, 2002.
40. Wachecka-Kotkowska, L.; Kotkowski, P. Grain-size distribution analysis of Quaternary sediments from the southern part of the Lodz region in Poland: A computational-methods approach. *Geologos* **2011**, *17*, 205–219. [CrossRef]
41. Feng, G.; Sharratt, B.S. Evaluation of the SWEEP model during high winds on the Columbia Plateau. *Earth Surf. Process. Landf.* **2009**, *34*, 1461–1468. [CrossRef]
42. Van Donk, S.J.; Skidmore, E.L. Field experiment for evaluating wind erosion models. *Ann. Arid Zone* **2001**, *40*, 281–302.
43. Van Donk, S.J.; Skidmore, E.L. Measurement and simulation of wind erosion, roughness degradation and residue decomposition on an agricultural field. *Earth Surf. Process. Landf.* **2003**, *28*, 1243–1258. [CrossRef]
44. Van Donk, S.J.; Huang, X.; Skidmore, E.L.; Anderson, A.B.; Gebhart, D.L.; Prehodaz, V.E.; Kellogg, E.M. Wind erosion from military training lands in the Mojave Desert, California, USA. *J. Arid Environ.* **2003**, *54*, 687–703. [CrossRef]
45. Hagen, L.J. Evaluation of the Wind Erosion Prediction System (WEPS) erosion submodel on cropland fields. *Environ. Model. Softw.* **2004**, *19*, 171–176. [CrossRef]

46. Sharratt, B.; Feng, G.; Wendling, L. Loss of soil and PM_{10} from agricultural fields associated with high winds on the Columbia Plateau. *Earth Surf. Process. Landf.* **2007**, *32*, 621–630. [CrossRef]
47. Goossens, D.; Buck, B.J. Can BSNE (Big Spring Number Eight) samplers be used to measure PM_{10}, respirable dust, $PM_{2.5}$, and $PM_{1.0}$? *Aeolian Res.* **2012**, *5*, 43–49. [CrossRef]
48. Environmental Systems Research Incorporated (ESRI). *ArcGIS 10.0*; Environmental Systems Research Incorporated: Redlands, CA, USA, 2011.
49. Mirzamostafa, N.; Stone, L.R.; Hagen, L.J.; Skidmore, E.L. Soil Aggregate and Texture Effects on Suspension Components from Wind Erosion. *Soil Sci. Soc. Am. J.* **1998**, *62*, 1351–1361. [CrossRef]
50. Hagen, L.J. Fine particulates (PM_{10} and $PM_{2.5}$) generated by breakage of mobile aggregates during simulated wind erosion. *Trans. ASAE* **2004**, *47*, 107–112. [CrossRef]
51. US-EPA. *PM-10 Guideline Document*; EPA-452/R-93-008; Office of Air Quality Planning and Standards, United Stated Environmental Protection Agency: Research Triangle Park, NC, USA, 1993.
52. NOM Norma Oficial Mexicana. *Valores límites permisibles para la concentración de partículas suspendidas PM_{10} y $PM_{2.5}$ en el aire ambiente y criterios para su evaluación [Environmental Health. Air Quality Standards for PM_{10} and $PM_{2.5}$ Particles in Ambient Air and Criteria for Evaluation]*; NOM-025-SSA1-2014 Salud Ambiental; Secretaría de Salud: México, D.F., México, 2014.